Food Bioscience 60 (2024) 104448

Contents lists available at ScienceDirect

Food Bioscience

journal homepage: www.elsevier.com/locate/fbio

Interfacial kinetics reveal enzymatic resistance mechanisms behind granular starch with smooth surfaces

Yu Wang [a,1], Yu Tian [b,1], Zhihang Li [b], Jacob Judas Kain Kirkensgaard [c,d], Birte Svensson [a,**], Andreas Blennow [b,*]

[a] Enzyme and Protein Chemistry, Department of Biotechnology and Biomedicine, Technical University of Denmark, DK-2800, Kgs. Lyngby, Denmark
[b] Department of Plant and Environmental Sciences, University of Copenhagen, DK-1871, Frederiksberg C, Denmark
[c] Department of Food Science, University of Copenhagen, DK-1958, Frederiksberg C, Denmark
[d] Niels Bohr Institute, University of Copenhagen, DK-2100, Copenhagen Ø, Denmark

ARTICLE INFO

Keywords:
Starch granule
Catalytic surface
Enzymatic resistance
Interfacial kinetics
Structure-catalysis relationship

ABSTRACT

Heterogeneous (interfacial) enzyme catalyzed hydrolysis of starch granules occurs in various biological systems, including plants, animal/human digestion, and microorganisms. Factors such as granular size, surface area, pores, and smoothness play crucial roles in influencing this process. However, limited understanding persists regarding the high enzymatic resistance of starch granules with smooth surfaces. In this study, we investigated the hydrolysis mechanism of glucoamylase (GA) on three different types of starch granules with smooth surfaces, extracted from *Curcuma zedoaria* (zedoary) rhizomes, *Solanum tuberosum* (potato) tubers, and *Manihot esculenta* (tapioca or cassava) roots. We compared the *Langmuir* adsorption, interfacial kinetics, and the multi-level structure of the three starches. Our data demonstrate that the lower enzymatic resistance observed in tapioca starch stems from the higher density of enzymatic attack sites ($^{kin}\Gamma_{max}$) recognized by GA on tapioca starch (1.0 nmol/g) compared to potato (0.6 nmol/g) and zedoary (0.3 nmol/g) starch granules. The high $^{kin}\Gamma_{max}$ for tapioca starch was significantly influenced by its relatively lower B-type crystallinity, which is disrupted by the presence of short fa chains (degree of polymerization (DP) < 12) and long amylose chains. Furthermore, the relatively higher proportion of longer chains (fb_1 and fb_2 chains) on the surface of tapioca starch also contributed to higher $^{kin}\Gamma_{max}$ for GA, resulting in lower enzymatic resistance. These findings enhance our understanding of how the structure of starch granules affects enzymatic catalysis, particularly in granular starches with smooth surfaces devoid of pores. Such insights are crucial for elucidating the digestion and utilization of starch granules.

1. Introduction

Starch, an abundant and renewable polysaccharide ubiquitous in plants, plays indispensable roles across various domains, notably in food production. However, its versatility extends beyond the culinary realm, with applications spanning biodegradable polymers, wastewater treatment, functional nanomaterials, and as a nutritional constituent in food formulations (Chi et al., 2021; Fang et al., 2022; França et al., 2022; Ren et al., 2020). Traditionally, starch undergoes gelatinization through cooking and heat-moisture processes, facilitating its utilization in diverse applications (Liu et al., 2020; Zhong et al., 2022). Yet, the escalating focus on sustainability and energy efficiency is driving interest in harnessing raw starch granules, guiding in novel applications, such as preparation of new RSII by modifying the surface structure, developing starch-based delivery systems for dietary supplements, and improving the digestibility of raw starch in animal feed through enzymatic treatment, which can enhance the nutritional value and energy efficiency for livestock (Liu et al., 2020, 2024; Situ et al., 2014; Zhong et al., 2021a; Zhong et al., 2021b; Zhu et al., 2016, 2024). To impart starch with novel functionalities and enhance its beneficial properties, there is a growing exploration of employing various hydrolases or transglycosylases to modify granular starches (Guo et al., 2019; Miao & BeMiller, 2023; Zhong et al., 2022). Of special nutritional interest is, that granular starch is categorized as so-called type II resistant starch

* Corresponding author.
** Corresponding author.
E-mail addresses: bis@bio.dtu.dk (B. Svensson), abl@plen.ku.dk (A. Blennow).
[1] These authors contributed equally to this work.

https://doi.org/10.1016/j.fbio.2024.104448
Received 21 March 2024; Received in revised form 26 May 2024; Accepted 29 May 2024
Available online 31 May 2024

(RSII), typical from green banana, low-moisture bakery foods like muesli and biscuits, which generally retains its granular structure, as well as high amylose starches that do not gelatinize efficiently (Kulp et al., 1991; Rosado et al., 2020; Wang et al., 2022). Novel very-high amylose starch types are now developed, such as the amylose-only barley starch having gelatinization temperature well above 100 °C (Carciofi et al., 2012). RSII has garnered increasing importance in managing glycemic levels and addressing associated lifestyle-related concerns, primarily as an effect of the low enzyme accessibility limited by the semi-crystalline structures (Lee et al., 2018; Pinhero et al., 2016; Zhang et al., 2015). However, only recently, the mechanisms behind enzymatic digestion of granular starches in foods was started to be explored (Tian, Wang, Liu, et al., 2023).

Starch displays specific features at different levels: At the molecular level, it is characterized by the linear α-1,4-glucan known as amylose (AM) and the branched α-1,4; α-1,6 glucan termed amylopectin (AP). At a higher level of molecular order, X-ray diffraction reveals crystalline and amorphous lamellae of about 8–11 nm. At yet a higher level, alternating layers of amorphous and semi-crystalline growth rings appear at around 0.1–0.4 μm thickness. Starch granular size ranges from 1 to 100 μm, as influenced by its botanical source (Pérez & Bertoft, 2010). However, our understanding of the molecular-level interactions between digestive enzymes and starch granules (Baldwin et al., 2015) is limited due to the lack of knowledge about the surface structures of the granules at the molecular and higher levels. For instance, the "blocklet" structure, observed through AFM, varies in size and organization across different starches, yet quantifying its influence on enzymatic resistance remains a subject of study (Baldwin et al., 2015). Additionally, the extent to as how flexible chains protruding from solvent-exposed surfaces interact with hydrolytic enzymes, such as α-amylase, presents challenges in terms of their molecular structure like chain length and branching (Baldwin et al., 2015). However, appropriate protocols to precisely determine the amounts, densities and structures of these flexible glucan chains and how these chains feature influence on enzyme binding and catalysis remains to be solved. While some studies have highlighted the importance of surface structural features in starch granule digestion (Li et al., 2018; Shrestha et al., 2012), determining these features and their relationship with enzyme reactions is complex and requires further research.

The digestion of starch granules in the human digestive tract entails the action of several hydrolases. These include salivary and pancreatic α-amylases (Glycoside Hydrolase family 13 (GH13)), as well as the intestinal brush border α-glucosidase, maltase-glucoamylase, and sucrase-isomaltase from GH31 (Cerqueira et al., 2020; Sim et al., 2008, 2010). Porcine pancreatic α-amylase and glucoamylase (GA, GH15) from *Aspergillus niger* (with the commercial name amyloglucosidase) are commonly used to mimic *in vitro* starch digestibility. Despite the similar exo-acting mode of GA and α-glucosidases, they operate differently. GA features an $(\alpha/\alpha)_6$ barrel catalytic domain and is an inverting enzyme releasing β-D-glucose, while the α-glucosidases have a $(\beta/\alpha)_8$ barrel catalytic domain and use a retaining mechanism, yielding α-D-glucose (Okuyama, 2011; Sierks et al., 1990).

Enzymatic catalysis on starch can be classified into two distinct situations: homogeneous catalysis, which involves gelatinized starch where both the substrate and enzyme are in solution, and heterogeneous (interfacial) catalysis, which pertains to insoluble starch granules (Tian, Wang, Zhong, et al., 2023; Wang et al., 2024). The interfacial catalysis poses a unique challenge as the molar concentration of the substrate cannot be precisely defined, given the insoluble nature of the granules (Kari et al., 2017). Tsatsumi et al. analyzed the hydrolysis kinetics of raw starch granules by glucoamylase using conventional and inverse kinetics separately (Tatsumi & Katano, 2005). Recently, as inspired by heterogenous catalysis of cellulases acting on cellulose, we analyzed the interfacial catalysis by combining conventional Michaelis-Menten kinetics, where substrate is in excess, with an inverse kinetics approach having the enzyme in excess, and with *Langmuir* adsorption isotherms to extract densities of enzyme attack- and binding sites on the surface of per gram of starch granules (Tian, Wang, Zhong, et al., 2023; Wang, Tian, et al., 2023). Our results showed that the lower enzymatic resistance of A-type crystalline polymorphic waxy (high amylopectin) and normal maize starch granules than B-type high-amylose maize starch granules stems from the higher density of attack sites (Tian, Wang, Liu, et al., 2023).

The starch granule surface functions as the primary substrate for starch-active enzymes, and the various granule surface features are crucial for the heterogeneous catalytic process. These features include surface area (Warren et al., 2011), the presence of pores, the smoothness of the surface (Chen et al., 2016; Haiteng Li, Hemar, & Zhu, 2021; Shrestha et al., 2012), the number of flexible glucan chains on the granule surface, and the "local polymer organization" (Baldwin et al., 2015; Dhital et al., 2014). Our previous study proposed that minimal presence of pores and cracks on the granular surface, as observed in, for example, high amylose starches and potato starch, is a key factor contributing to their high enzymatic resistance. Particularly, for normal potato starch granules, its notably smooth surface acts as an effective barrier against enzyme access to the granule interior, resulting in the lowest enzymatic degradation percentage found (Blennow et al., 2003; Jung et al., 2013; Tian et al., 2024). However, whether the smooth surface solely dictates enzymatic resistance remains uncertain. Several natural starches, such as sweet potato-, banana-, zedoary-, and tapioca starch granules, exhibit smooth surfaces similar to potato starch (Abegunde et al., 2013; Jane et al., 1994; Pokharel et al., 2023; Xiao et al., 2018). In spite of this shared smooth granular surface feature without noticeable pores and cracks, apart from the smooth surface, the structural features influencing the enzymatic resistance of these starch granules remains to be identified.

In this study, we collected three common starch varieties known for their smooth surfaces from *Curcuma zedoaria* (zedoary) rhizomes, *Solanum tuberosum* (potato) tubers, and *Manihot esculenta* (tapioca or cassava) roots. Using an interfacial kinetics approach, we quantified the productive and unproductive binding sites of *Aspergillus niger* glucoamylase (GA) on these distinct surfaces. Combining with the structural analysis, our goal is to offer a thorough understanding of the enzymatic resistance mechanisms for granular starches featuring smooth surfaces.

2. Materials and methods

2.1. Starch and enzyme sources

Three different starch granular types were isolated from *Curcuma zedoaria* (zedoary) rhizomes, *Solanum tuberosum* (potato) tubers, and *Manihot esculenta* (tapioca or cassava) roots. (Blennow et al., 2005; Vamadevan et al., 2018). Glucoamylase (GA) from *Aspergillus niger* (A7095) and pancreatin from porcine pancreas (P7545) were purchased from Sigma-Aldrich (USA), and the molecular weight (M_w) of GA was 75 kDa. Pullulanase M2 from *Bacillus licheniformis* (E-PULBL, 900 U/mL) was purchased from Megazyme Co. Ltd (Wicklow, Ireland).

2.1.1. Scanning electron microscopy (SEM)

The granule morphology and surface topography was determined by affixing the starch granules to carbon tapes on aluminum SEM stubs followed by coating with 6 nm of gold using a Leica EM ACE200 gold coater (Leica Microsystems, Wetzlar, Germany). The samples were scanned with a field emission scanning electron microscope (FE-SEM) on an FEI Quanta 200 microscope at magnifications of 5000 × , following established protocols.

2.2. Size-exclusion chromatography (SEC)

The chain length distributions (CLDs) of starch granules post-pullulanase debranching were analyzed using a Size Exclusion Chromatography-Triple Detector Array (SEC-TDA) system equipped

with a GRAM pre-column and GRAM1000 connected to a TDA302 detection array (Viscotek, Malvern, UK). Differential refractive index (DRI) signals were recorded using a refractive index detector (PN3140, PostNova Analytics, Landsberg, Germany), and data were analyzed using PSS WinGPC Unity software (Polymer Standard Services, Mainz, Germany) (Tian et al., 2024).

For native starch analysis, 5 mg samples were dissolved in 1 mL DMSO/LiBr (0.5% w/w) at 80 °C overnight, and injected into the SEC system, without filtering before injection to avoid shear degradation (Cave et al., 2009; Xu et al., 2024; Zhang et al., 2021). Elution was carried out with DMSO/LiBr at 0.5 mL/min and 65 °C. Pullulanase debranched samples were prepared by heating starch dispersion in DMSO/LiBr, followed by centrifugation (4000 *g*, 10 min), ethanol precipitation, and freeze-drying. The freeze-dried sample (50 mg) was suspended in 1 mL sodium acetate buffer (10 mM, pH 4.0), gelatinized (99 °C, 30 min) and debranched by adding pullulanase (final concentration: 50 nM) and incubated at 40 °C for 3 h. The resulting debranched samples were dissolved in DMSO/LiBr for analysis (Li et al., 2016).

2.3. High-performance anion exchange chromatography-pulsed amperometric detection (HPAEC-PAD)

For CLD analysis on the granular surface, starch granules (50 mg/mL, w/v), resuspended in 50 mM sodium acetate pH 5.5, was debranched by 50 nM (final concentration) pullulanase (25 °C, 30 min), followed by centrifugation (10,000 *g*, 5 min) (Wang et al., 2024). For CLD analysis of gelatinized starches, starch (5 mg/mL), resuspended in 50 mM sodium acetate pH 5.5, was gelatinized (99 °C, 30 min) and then debranched by 50 nM pullulanase (40 °C, 3 h). Subsequently, the debranched starch (40 μL, 5 mg/mL) was injected onto a CarboPac PA-200 column connected to an HPAEC-PAD system (Dionex, Sunnyvale, CA, USA). Columns were initially rinsed with 100 mM NaOH at a flow rate of 0.4 mL/min for 20 min. Elution utilized three solvents: MilliQ water (eluent A), 1 M NaOH (eluent B), and 1 M NaOH enriched with 25 mM NaAc (eluent C). The elution gradient proceeded as follows: an initial phase from 0 to 5 min (15% eluent A and 85% eluent C), followed by 5–130 min (linear increase of eluent B to 40% and linear decrease of eluent C to 45%), 130–135 min (80% eluent A and 20% eluent C), and finally, 135–145 min (returning to the original eluent mixture). Peak integration and detector response were conducted as previously described (Blennow et al., 1998).

2.4. Wide-angle X-ray scattering (WAXS)

Starch granules were exposed in a closed container containing a saturated aqueous solution of NaCl for 2 weeks before analyzing crystalline allomorphs and relative crystallinity. The analysis utilized a Nano-inXider instrument (Xenocs SAS, Grenoble, France) with a Cu-Kα radiation. Radially averaged intensity (I) was plotted against scattering angle (2θ) between 5 and 40° using a wavelength of 0.1542 nm. Relative crystallinity was calculated following established methods by using the PeakFit software (version 4.12) (Brückner, 2000).

2.5. Particle size analysis

The particle size and surface area of starches were assessed using the Mastersizer 3000 laser particle size analyzer (Malvern Instruments Ltd, Worcestershire, U.K). The average particle size was expressed by the volume mean diameter (D (4,3)). The specific surface area (SSA) per unit weight of the particles was calculated by assuming a specific gravity of 1.5 (Warren et al., 2011).

2.6. Fourier transform infrared-attenuated total reflectance (FTIR-ATR) spectroscopy

Starch samples were equilibrated to around 50% relative humidity (RH) before analysis. Spectral data were acquired using a Bomem MB100 FTIR spectrometer (ABB-Bomem, Quebec, Canada) equipped with a Golden gate attenuated total reflectance (ATR) accessory. Spectra for each sample were combined by co-adding at a resolution of 4 cm^{-1}, with a background spectrum collected through 128 co-added scans. A Lorentzian line shape with a half-width of 19 cm^{-1} and a resolution enhancement factor of 1.9 was assumed. Following baseline correction and deconvolution, IR absorbance values at 1022 cm^{-1} and 1045 cm^{-1} were extracted from the spectra using OMNIC software (Capron et al., 2007).

2.7. In vitro digestibility

The starch granules were subjected to *in vitro* digestion (Tian et al., 2021). Starch granules (20 mg) were suspended in 2 mL of 50 mM sodium acetate, 5 mM $CaCl_2$ at pH 5.5, preheated (37 °C, 10 min) and incubated with pancreatin (2 mg/mL, final concentration) and glucoamylase (3.6 μM, final concentration) at 37 °C, 1100 rpm for 2 h. Aliquots (50 μL) were withdrawn at 0, 10, 20, 30, 40, 60, 90, 120, and 180 min, mixed with 95% ethanol (500 μL), and centrifuged (10,000 *g*, 5 min). Glucose in the supernatant was quantified using the GOPOD assay (D-Glucose Assay Kit, Megazyme), with glucose as a standard (Huggett, 1957). Resistant starch (RS) was defined as the percent weight of starch remaining residue after 120 min.

2.8. Langmuir adsorption of starch granules

The binding capacities were assessed at 37 °C using 0.1 mg/mL of acarbose (A8980, Sigma-Aldrich, Milano, Italy) to inhibit GA activity, thus ensuring no alteration of the starch granule surface during testing (Tian, Wang, Liu, et al., 2023). A consistent starch granule load of 15 mg/mL was employed, while the enzyme concentration ranged from 6.8 to 1370 nM. Following a 10 min incubation period (37 °C, 1100 rpm), the mixtures were centrifuged (10,000 *g*, 5 min), and 100 μL of supernatant was mixed with 100 μL of 2.5-fold diluted Protein Assay Dye Reagent (Bio-Rad). Enzyme concentration in solution (E_{free}) was determined by measuring absorbance ratios at 590 nm and 450 nm, using Bovine Serum Albumin (BSA, Sigma) as standards. The data were analyzed using GraphPad Prism 6 (GraphPad Software Inc) and fitted to the *Langmuir* isotherm (eq. (1)), where K_d represents the dissociation constant and ${}^{ads}\Gamma_{max}$ denotes the (apparent) saturation coverage (Kari et al., 2017).

$$\Gamma = \frac{{}^{ads}\Gamma_{max} \bullet E_{free}}{K_d + E_{free}} \quad (1)$$

2.9. Interfacial kinetics analysis on granular starch

Two complementary methods, conventional and inverse Michaelis-Menten (MM) analyses, were employed to characterize the kinetics of granular starch hydrolysis. For the conventional MM analysis, starch granules (135 μL, 15–150 mg/mL) were pre-incubated (37 °C, 10 min, 1100 rpm) and the reaction was initiated by addition of GA (15 μL, final concentration 0.7 nM), followed by further incubation (37 °C, 1100 rpm, 10 min). In the case of inverse MM kinetics analysis, starch granules (135 μL, 15 mg/mL) were mixed with 20 μL of seven GA concentrations (0.7–171 nM, final concentrations). After 30 min, aliquots (100 μL) were transferred to new tubes, mixed with 20 μL of 1.8 M Na_2CO_3 to terminate the reaction, centrifuged (10,000 *g*, 5 min), and the concentration of reducing sugar in the supernatant was determined using the PAHBAH method (Lever et al., 1973).

Conventional MM data were analyzed using eq. (2) for non-linear regression analyses where S_0^{mass} is the substrate mass load and $K_{1/2}$ (in $g{\cdot}L^{-1}$) is the mass load at substrate half-saturation and V_{max} (in $M{\cdot}s^{-1}$) is the maximum rate for conventional kinetics (Kari et al., 2017).

$$v_0 = \frac{V_{max} \cdot S_0^{mass}}{K_{1/2} + S_0^{mass}} \quad (2)$$

The inverse experiments we analyzed using the inverse MM equation (eq. (3)) by nonlinear regression analysis where E_0 is the enzyme load and $^{inv}K_M$ (in M) is the enzyme concentration at enzyme half-saturation and $^{inv}V_{max}$ (in $g \cdot L^{-1} \cdot s^{-1}$) is the maximum rate for inverse kinetics.

$$v_0 = \frac{^{inv}V_{max} \cdot E_0}{^{inv}K_M + E_0} \quad (3)$$

The attack site density ($^{kin}\Gamma_{max}$) was calculated by eq. (4) using V_{max} (eq. (2)) and $^{inv}V_{max}$ (eq. (3)) (Kari et al., 2017).

$$\frac{\frac{^{inv}V_{max}}{S_0^{mass}}}{\frac{V_{max}}{E_0}} = {}^{kin}\Gamma_{max} \quad (4)$$

2.10. Statistical analysis

Interfacial kinetics was analyzed in duplicate and all other experiments in triplicate. The statistical significance was assessed with one-way analysis of variance (ANOVA) using SPSS 20.0 (SPSS Inc., Chicago, USA). p values of <0.05 were considered statistically significant throughout the study. The correlations were analyzed using Pearson correlation through the "cor" function and visualized using the R package "corrplot" (Wei et al., 2017).

3. Result and discussion

3.1. Granular morphology

The granule shape of zedoary starch appeared to be a flaky oval or elliptic (Braga et al., 2006; Policegoudra & Aradhya, 2008) and potato granules showed regular and spherical granules (Fig. 1) (Blennow et al., 2003; Hua Li, Hemar, & Zhu, 2021). The granules of tapioca starch were sphere-shaped or ellipsoid-shape with one or more spherical truncations (Prompiputtanapon et al., 2020). Even though the SEM images revealed significant variations in shape and size between zedoary, potato, and tapioca starches, all these three showed a smooth surface without pores and cracks.

3.2. Chain length distributions (CLDs) as analyzed by SEC

The size distribution profiles of raw starches, analyzed by SEC, revealed two distinct populations: population I (Hydrodynamic radius (Rh) $>$ 66 nm), identified as the amylopectin (AP) fraction, and population II (Rh $\leq$ 66 nm), known as the amylose (AM) fraction (Tian et al., 2024; Vilaplana & Gilbert, 2010). Zedoary and potato starches exhibited a significant peak around 115 nm in population I, whereas tapioca starch displayed a major peak at 100 nm, indicating a smaller AP molecule size compared to zedoary (114.8 nm) and potato (116.3 nm) starches. Concerning the AM fractions, potato starch (13.9 nm) demonstrated a smaller AM molecule size compared to zedoary (15.7 nm) and tapioca (16.2 nm) starches (Fig. 2 and Table 1).

The compositional length distribution profiles of debranched starches, analyzed by SEC, displayed three populations: population I (DP 6–30), population II (DP 31–200), and population III (DP $>$ 200), categorized as short AP chains (AP1), long AP chains (AP2), and AM chains, respectively (Tian et al., 2024; Yu et al., 2019). The AP chains, including AP1 and AP2, were predominant in all three starches. Specifically, the AP1 population dominated in zedoary and tapioca starches, while the AP2 population dominated in potato starch. Among the three starches, the potato starch exhibited the highest AM content ($RC_{de\text{-}AM}$) and tapioca starch showed the longest ACL $_{de\text{-}AM}$.

3.3. Chain length distributions (CLDs) as analyzed by HPAEC-PAD

The CLD profiles of gelatinized starches as monitored by HPAEC-PAD analysis (Fig. 3 and Table 2) primarily depicted detailed variations in AP structure and AM short-chain decorations. To distinguish these differences clearly, the chains were divided into four subfractions: fa (DP 6–12), fb_1 (DP 13–24), fb_2 (DP 25–36), and fb_3 (DP $>$ 36) (Bertoft, 2017). The data revealed that: (i) across all three starches, tapioca starch exhibited higher amounts of short fa chains (DP 6–12) and lower amounts of long chains (fb_2 and fb3 chain) compared to the other starches; (ii) Potato starch displayed a slightly lower content of fb_1 chains (DP 13–24) and higher amounts of fb_3 chains (DP $>$ 36) (Table 2). Considering both the $Rh_{na\text{-}AP}$ (Table 1) and CLD (Table 2), the higher proportion of short chains and lower proportion of long chains in tapioca starch resulted in a smaller AP molecule size compared to the other two starches.

In our previous study, pullulanase was used to hydrolyze branches on the surface of starch granules. The condition for the CLD analysis of the surface of starch granules, such as the starch and enzyme concentration, and reaction time is based on Michaelis–Menten kinetics principles. Under this circumstance, the surface-debranching of starch granule by *Bl*Pul was within the linear time and enzyme concentrations range necessary for the Michaelis-Menten steady state assumption (Kari et al., 2020; Schnell, 2014). To secure robustness of the method, we chose different conditions for the CLD analysis within the linear range of MM kinetics, and we constantly got similar CLD patterns. Besides, the SEM images demonstrated that no pores or cracks were generated by *Bl*Pul on the surface of starch granules under the test conditions, confirming that the hydrolysis of starch granules by *Bl*Pul only took place on the surface (Wang et al., 2024). Consequently, the products generated by pullulanase hydrolysis from starch granules can serve as an estimation of the CLD on the surface of starch granules. Hence, the chain length of the starch granules surface was also analyzed (Fig. 3B–D, and F, and Table 2). Zedoary and potato starches showed a higher proportion of short chain (fa chains, DP 6–12) and less long chains (fb_1 and fb_2 chain)

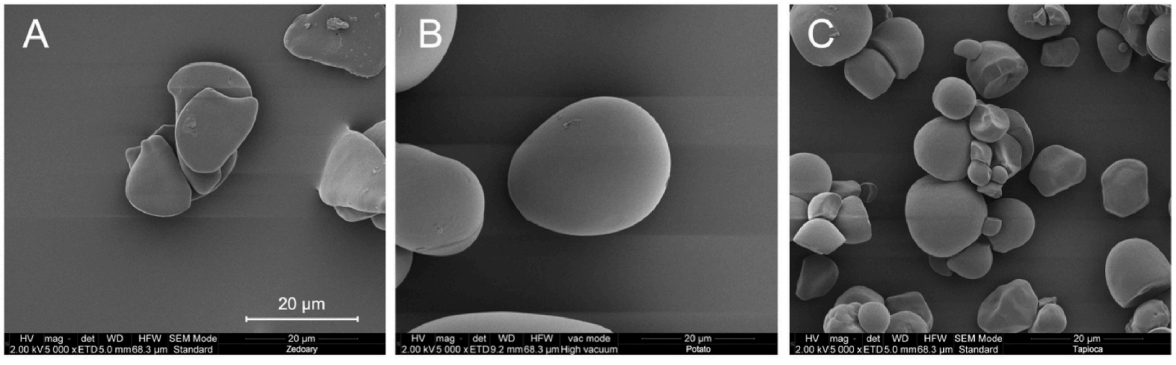

Fig. 1. SEM images of three starch granules. (A) zedoary starch, (B) potato starch, and (C) tapioca starch. Magnification is 5000×.

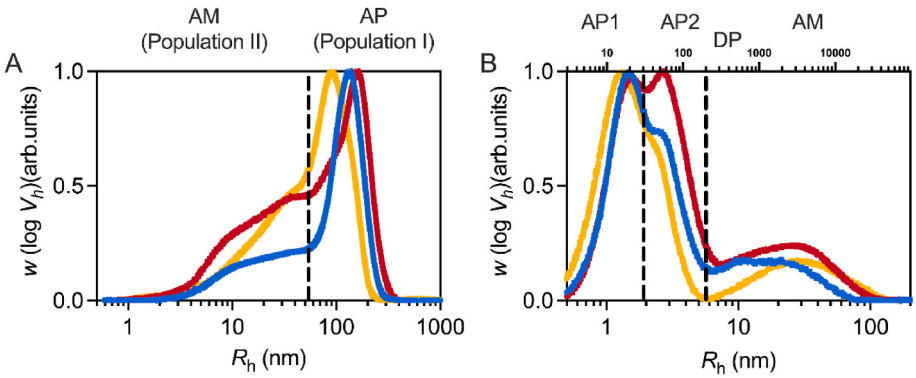

Fig. 2. SEC weight distributions of whole (fully branched) starch molecules (left) and chain length distribution obtained by SEC analysis of debranched starch molecules (right) of zedoary starch (blue), potato starch (red), and tapioca starch (yellow).

Table 1
The changes of average chain lengths (ACL) of debranched AP and AM fractions of three starches.

Starch	Zedoary	Potato	Tapioca
$RC^{1}_{de\text{-}AP1}$ (%)	48.7 ± 2.3[2 b3]	37.4 ± 0.3[c]	59.2 ± 0.4[a]
$RC_{de\text{-}AP2}$ (%)	31.9 ± 2.3[b]	40.8 ± 0.1[a]	23.5 ± 0.2[c]
$RC_{de\text{-}AM}$ (%)	19.3 ± 0.1[b]	21.8 ± 0.4[a]	17.2 ± 0.6[c]
$ACL^{4}_{de\text{-}AP1}$	12.7 ± 0.9[ab]	14.3 ± 0.1[a]	10.8 ± 0.4[b]
$ACL_{de\text{-}AP2}$	63.7 ± 0.8[b]	68.8 ± 0.1[a]	54.7 ± 0.7[c]
$ACL_{de\text{-}AM}$	1140 ± 40[b]	1450 ± 20[b]	2020 ± 120[a]
$Rh^{5}_{na\text{-}APe}$ (nm)	114.8 ± 3.8[a]	116.3 ± 3.2[a]	100.0 ± 5.8[a]
$Rh_{na\text{-}AM}$ (nm)	15.7 ± 1.0[a]	13.9 ± 0.5[a]	16.2 ± 2.0[a]
$RC^{6}_{na\text{-}AP}$ (%)	65.1 ± 3.2[a]	55.4 ± 0.4[a]	59.1 ± 2.2[a]
$RC_{na\text{-}AM}$ (%)	34.9 ± 3.2[a]	44.6 ± 0.4[a]	40.9 ± 2.2[a]

1 RCde-X: relative amount of fraction X of debranched sample.
2 Values are means ± standard deviation.
3 Values with different letters in the same row are significantly different at $p < 0.05$.
4 ACLde-X: the average chain length (DP) of the fraction X of debranched sample.
5 Rhna-X: hydrodynamic radius of fraction X of native sample.
6 RCna-X: relative amount of fraction X of native sample.

on the surface compared to tapioca starches.

3.4. Multi-scale structures

Crystalline structure. The crystalline polymorphs as deduced from WAXS data (Fig. 4) showed that zedoary and potato starches displayed a typical B-type crystalline polymorph with signature peaks at 5.6°, 22.0°, and 24.0° 2θ. However, minor differences were detected, e.g., the double peak at 22° and 24° 2θ was sharper for the zedoary starch granules. Conversely, tapioca starches showed a mixture of A- and B-crystalline polymorph by showing a typical peak at 15° 2θ and a single peak at 23° 2θ significative for the A-type crystal, and a single peak at 17° and a characteristic peak at 5.6° 2θ for B-type crystal (Cai & Shi, 2014; Vamadevan et al., 2018; Zhang et al., 2018). The crystallinities of potato and cassava starch fractions (Table 3) show that the Zedoary starch (28.6%) had significantly higher crystallinity than potato starch (20.3%) and tapioca starch (16.6%). For tapioca starch, the A- and B-type crystallinities were 6.8% and 9.8%, respectively.

Surface order degree. The FTIR-ATR spectra of the three starch granules in the range of 800–1300 cm^{-1}, which corresponds to C–O and C–C stretching vibrations, provide insights into polymer conformation at the surface (~2 μm) of starch granules. The presence of ordered and amorphous regions is indicated by the observed bands at 1045 cm^{-1} and 1022 cm^{-1}, respectively. The ratio of 1045 cm^{-1}/1022 cm^{-1} is commonly employed to evaluate the degree of surface order in starch. The 1045 cm^{-1}/1022 cm^{-1} was found not related to the CLD on the surface of starch granules. Among the three starches studied here, tapioca starch exhibited the lowest degree of surface order (0.75) (Table 3).

Particle size and specific surface area. The volume-weighted mean diameter ($D_{4,3}$) and specific surface areas (SSA) are provided for three starches. Potato and tapioca starch exhibited larger D (4,3) values, approximately 37 μm and 31 μm respectively. Zedoary starch, on the other hand, also being pseudo-two-dimensional and flat, displayed a smaller granular size with 19 μm, and consequently, the largest specific surface area, measuring 370 m^2/kg.

3.5. In vitro digestibility

The digestibility of zedoary-, potato-, and tapioca starch were compared using an *in vitro* system containing pancreatin and GA (Fig. 5 and Table 3). Although all three starches exhibited significantly lower digestibility compared to starch granules with less-smoothed surfaces, such as those of maize, wheat, and barley (Tian et al., 2024), differences were observed among them. Tapioca starch showed the lowest enzymatic resistance, with a digestion percentage of 23.8% after 180 min, followed by potato starch at 9.6%, and zedoary starch exhibiting the lowest digestibility at 6.0%. Despite all three starch granules having smooth surfaces (Fig. 1), the variation in the degree of digestion after 180 min (C180) suggests that the smooth surface alone cannot be the sole factor influencing resistance to enzymatic degradation.

3.6. Langmuir adsorption of starch granules

The enzymatic reaction on starch granules can be divided into four processes: diffusion, adsorption, catalysis, and desorption (Tian, Wang, Zhong, et al., 2023). Hence, both binding affinity and catalytic ability of enzyme are crucial for the degradation of starch granules (Butterworth et al., 2022; Tatsumi et al., 2007; Warren et al., 2011).

Langmuir adsorption was used to determine the binding affinity and capacity. Firstly, it must be mentioned that acarbose was added to the enzyme solution to inhibit GA prior to the binding test. We are aware of that inhibition of GA might affect the binding behavior of GA to the starch granules. However, since GA showed very high activity on starch granules, we decided this method to be the best compromise to avoid changing the surface structure of starch granules by GA-assisted hydrolysis during the test (Tian, Wang, Liu, et al., 2023). GA showed similar affinity ($1/K_d$) for potato (0.013 nM^{-1}) and tapioca (0.012 nM^{-1}) starches, which was 4.3- and 4.0-fold higher, respectively, than for zedoary starch (0.003 nM^{-1}) (Fig. 6 and Table 4). The approximate values of the apparent saturation coverage of GA for the three different starch granule types was used to estimate the density of binding sites ($^{ads}\Gamma_{max}$) of GA on the different granular surfaces. GA recognized 2.7- and 2.2-fold more binding sites ($^{ads}\Gamma_{max}$) on zedoary starch (17.5

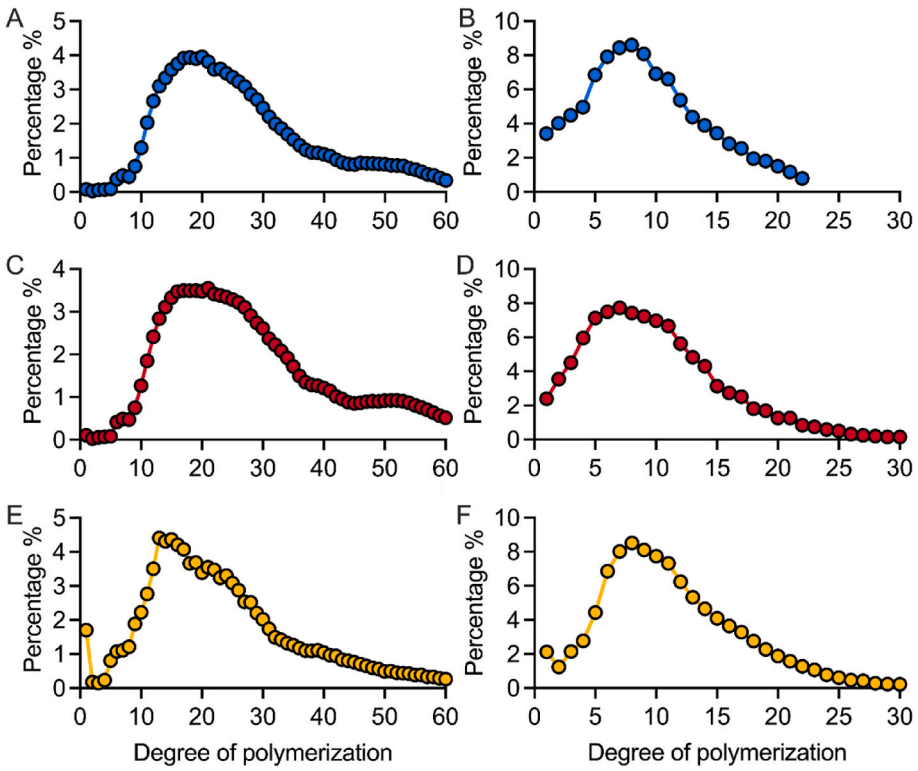

Fig. 3. Chain length distribution (CLD) of chains released by pullulanase-catalyzed debranching from granular and gelatinized starches. (A) Gelatinized and (B) granular zedoary starch, (C) gelatinized and (D) granular potato starch, and (E) gelatinized and (F) granular tapioca starch. Zedoary starch: blue, potato starch: red, and tapioca starch: yellow.

Table 2
Relative content of different branch chains in AP of three starches.

Samples		Type of chain[1]	Zedoary	Potato	Tapioca
Gelatinized starch	Average chain lengths (ACLs[2]) (DP)	fa	10.0 ± 0.2[3 a4]	9.9 ± 0.2[a]	8.4 ± 0.1[b]
		fb_1	18.6 ± 0.0[a]	18.6 ± 0.0[a]	18.1 ± 0.0[b]
		fb_2	29.5 ± 0.2[a]	29.7 ± 0.1[a]	29.4 ± 0.0[a]
		fb_3	46.6 ± 0.2[a]	47.1 ± 0.1[a]	45.6 ± 0.2[b]
Gelatinized starch	Relative proportions (RC^5_{de}) (%)	fa	8.4 ± 0.2[b]	8.0 ± 0.5[b]	16.9 ± 0.1[a]
		fb_1	44.0 ± 3.4[a]	40.4 ± 2.6[a]	45.7 ± 0.8[a]
		fb_2	28.4 ± 1.3[a]	29.7 ± 0.7[a]	23.7 ± 0.1[b]
		fb_3	19.4 ± 1.9[a]	22.0 ± 1.5[a]	15.5 ± 1.0[b]
Granular starch	Relative proportions (RCg^6) (%)	fa	75.7 ± 2.1[a]	72.7 ± 3.4[a]	65.5 ± 2.9[b]
		fb_1	24.2 ± 0.5[b]	25.7 ± 2.2[b]	32.6 ± 1.8[a]
		fb_2	ND[7]	1.6 ± 0.4[a]	2.2 ± 0.3[a]
		fb_3	ND	ND	ND

[1] fa: AP chains with DP < 12, fb_1: AP chains with DP 13–24, fb_2: AP chains with DP 25–36, fb_3: AP chains with DP > 36.
[2] ACLX: average chain lengths (DP) of fraction X of debranched gelatinized starch samples.
[3] Values are means ± standard deviation.
[4] Values in the same row with different letters are significantly different ($p < 0.05$).
[5] $RC_{de}X$: relative amount of fraction X of debranched gelatinized starch samples.
[6] RC_gX: relative amount of fraction X of debranched granular starch samples.
[7] ND: not detetected.

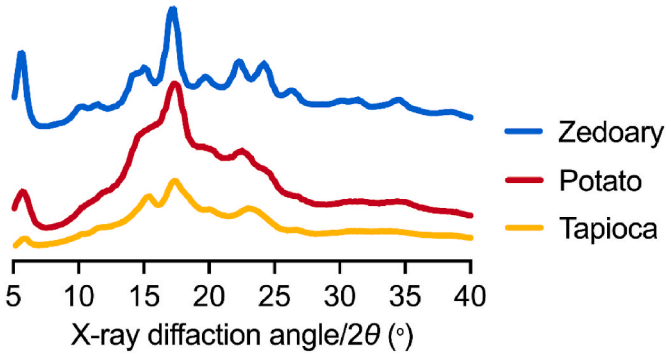

Fig. 4. WAXS diffractograms of zedoary (blue), potato (red), and tapioca starch (yellow) granules.

Table 3
Degree of branching, crystalline, FTIR peak ratios, particle size and digestion properties of the different B-type starches.

Starch	Zedoary	Potato	Tapioca
Crystallinity (%)	28.6 ± 0.5[1 a2]	20.3 ± 3.1[b]	16.6 ± 1.3[b3]
FTIR ratio[4] (1045/1022 cm^{-1})	0.81 ± 0.0[b]	0.87 ± 0.01[a]	0.75 ± 0.00[c]
$D^5_{4,3}$ (um)	19.2 ± 0.1[c]	37.4 ± 0.1[a]	31.0 ± 0.9[b]
Specific surface area (m^2/kg)	370 ± 1[a]	236 ± 0[c]	253 ± 6[b]
C^6_{180} (%)	6.0 ± 0.4[c]	9.6 ± 0.1[b]	23.8 ± 0.9[a]

1 Values are means ± standard deviation.
2 Values with different letters in the same row are significantly different at p < 0.05.
3 Tapioca starch is a mixture with A (6.8%) and B (9.8%) type crystals.
4 FTIR ratio: the ratio of 1045 cm−1/1022 cm−1from the FTIR-ATR spectra.
5 D4,3: the volume-weighted mean diameter.
6 C180: degree of digestion after 180 min.

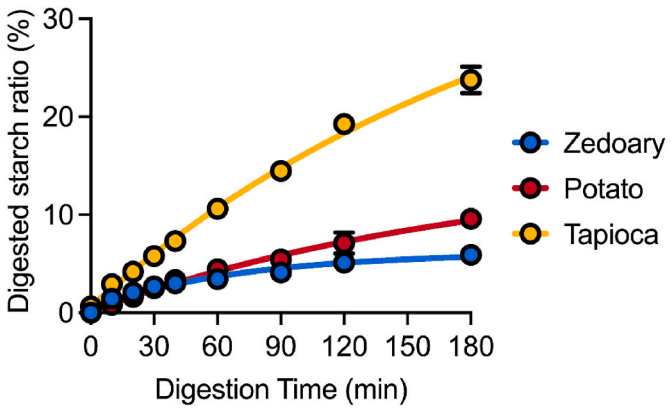

Fig. 5. *In vitro* digestion of zedoary starch (blue), potato starch (red), and tapioca starch (yellow).

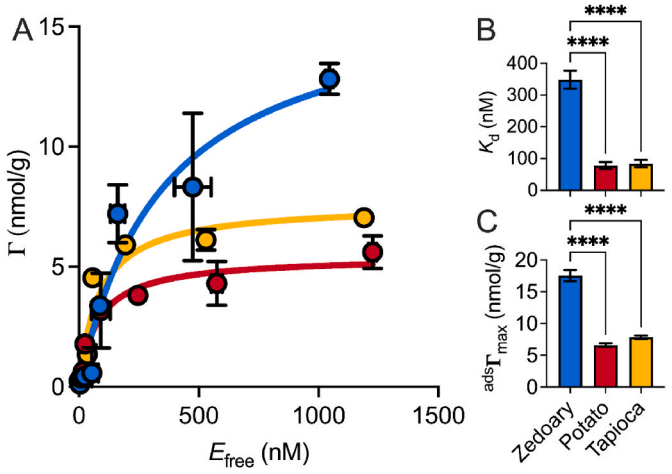

Fig. 6. *Langmuir* adsorption for GA on zedoary starch (blue), potato starch (red), and tapioca starch (yellow). (A) Binding isotherms. Lines represent best fits of the *Langmuir* equation (eq. (1)). (D) K_d, and (E) $^{ads}\Gamma_{max}$. **** represent statistical significance with p value < 0.0001.

Table 4
Langmuir adsorption and interfacial kinetic parameters of GA acting on zedoary, potato, and tapioca starch granules.

Starch	Zedoary	Potato	Tapioca
K_d^1 (nM)	349 ± 28[2] [a3]	78.3 ± 10.5[b]	83.7 ± 11.9[b]
$^{ads}\Gamma_{max}$[4] (nmol/g)	17.5 ± 0.7[a]	5.7 ± 0.2[b]	7.8 ± 0.2[b]
k_{cat}^5 (s^{-1})	58.7 ± 5.2[a]	52.3 ± 3.9[a]	60.2 ± 6.4[a]
$K_{1/2}^6$ (g/L)	46.1 ± 3.5[a]	54.0 ± 4.1[a]	30.8 ± 4.6[a]
$k_{cat}/K_{1/2}^7$ (L•[g•s]$^{-1}$)	1.3 ± 0.0[a]	0.8 ± 0.0[a]	2.0 ± 0.1[a]
$^{kin}\Gamma_{max}$h[8] (nmol/g)	0.3 ± 0.0[c]	0.6 ± 0.0[b]	1.3 ± 0.1[a]
A/B ratio[9] (%)	1.8 ± 0.1[b]	11.1 ± 0.3[a]	13.2 ± 1.0[a]

1 Kd: binding affinity.
2 Values are means ± standard deviation.
3 Values with different letters in the same row are significantly different at p < 0.05.
4 adsGmax: density of binding sites.
5 kcat: turnover number from conventional kinetics.
6 K1/2: the mass load at substrate half-saturation from conventional kinetics.
7 kcat/K1/2: catalytic efficiency from conventional kinetics.
8 kinGmax: density of attack sites.
9 A/B ratio: Attack site density/binding site density ratio.

nmol/g) when compared with potato starch (5.7 nmol/g) and tapioca starch (7.8 nmol/g) (Fig. 6E and Table 4).

3.7. Interfacial kinetics of starch granules

The interfacial hydrolysis of different starch granules by GA was analyzed using a combination of conventional and inverse MM kinetics (Fig. 7A and B) (Kari et al., 2017; Wang, Svensson, et al., 2023). Among the three different granular starch types, tapioca starch showed the highest k_{cat} (60.2 s^{-1}) and lowest $K_{1/2}$ (30.8 g/L), and therefore highest $k_{cat}/K_{1/2}$ (2.0 L•[g•s]$^{-1}$) using conventional MM kinetics (Table 4), hence, tapioca starch was more efficient substrate for GA among these three starches. Importantly, the combination of conventional and inverse MM kinetics permitted to determine the density of attack sites ($^{kin}\Gamma_{max}$). Our present findings reveal that GA has 4.3- and 2.2-fold more attack sites ($^{kin}\Gamma_{max}$) on tapioca starch (1.3 nmol/g) compared to zedoary (0.3 nmol/g) and potato (0.6 nmol/g) starches (Table 4).

Another important parameter derived from the interfacial kinetics and *Langmuir* adsorption is the attack site density/binding density site ratio (A/B ratio), which represents the proportion of productive binding density of GA for the different granular surfaces. Interestingly, only 1.8% of binding sites GA recognized on zedoary starch were productive, which was significantly lower than for potato (11.1%) and tapioca (13.2%) starches (Table 4).

4. Discussion

To explore deeper into factors influencing enzymatic resistance, we conducted a correlation analysis of three starch granule structural parameters and their interfacial kinetics and digestibility (Fig. 8).

Firstly, the smooth granular surface without pores and cracks acts as an efficient barrier for limiting enzyme binding, as supported by the significantly lower density of binding sites of the three starches compared with e.g. maize starch (Tian, Wang, Liu, et al., 2023). GA had lowest affinity for zedoary starch (K_d of 349 nM, Table 4), and zedoary starch showed the lowest *in vitro* digestibility (Fig. 5). In comparison, GA had highest affinity for potato starch (K_d of 78.3 nM, Table 4), but potato showed moderate *in vitro* digestibility (Fig. 5). Therefore, it can be concluded that for starches with the smooth granular surfaces, the binding step is not the limitation for the different enzymatic resistance (Fig. 8) as there is no correlation between binding affinity ($1/K_d$) or density of binding sites ($^{ads}\Gamma_{max}$) and digestibility (C180) (Fig. 8). The density of binding sites ($^{ads}\Gamma_{max}$) was positively related to the specific surface area (SSA), that is, larger area provided more substrate for enzyme, in agreement with a previous study (Jung et al., 2013). As for the binding affinity ($1/K_d$), our results demonstrated that the SSA of granular starch has a negative effect on the $1/K_d$ of GA (Fig. 8), which also is in line with previous studies for α-amylase (Warren et al., 2011). Interestingly, it should be noted that GA showed the lowest binding affinity ($1/K_d$), but the highest $^{ads}\Gamma_{max}$ to zedoary starch, indicating that the binding sites on the surface of zedoary starch granule are not as efficient as on potato and tapioca starch. The weak binding may also cause lower $^{kin}\Gamma_{max}$ for GA on zedoary starch.

Enzyme adsorption alone does not necessarily lead to catalysis. For these three starch granules having smooth surfaces, the density of attack sites ($^{kin}\Gamma_{max}$) is negatively correlated to digestibility (Fig. 8). Besides, it was also found that starches with higher B-type crystallinity showed a lower value of $^{kin}\Gamma_{max}$. Our former study also reported that low $^{kin}\Gamma_{max}$ for B-type high amylose maize starch was leading to higher enzymatic resistance than A-type waxy (high amylopectin) and normal maize starches (Tian, Wang, Liu, et al., 2023). It has been widely accepted that B-type crystals tend to form larger 100 nm-sized "blocklets" at the granule surface, which are believed to play a crucial role in conferring resistance to hydrolysis (Pérez & Bertoft, 2010). It was suggested that the short branches (fa chains, DP < 12), which are relatively higher in amount in tapioca starch, are too short to effectively participate in

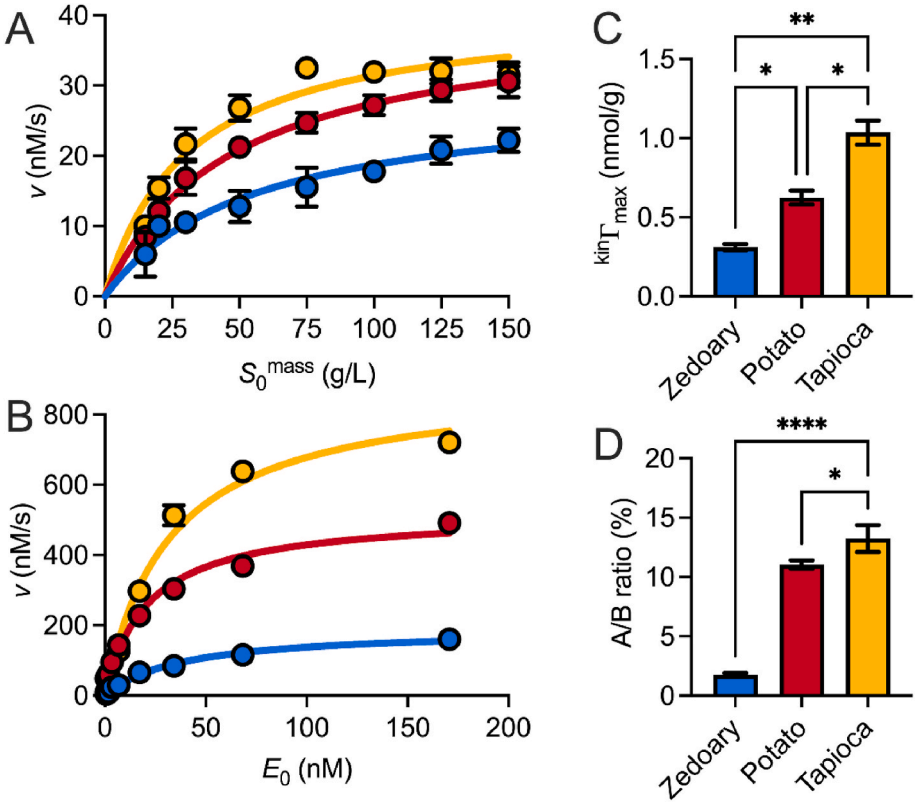

Fig. 7. Interfacial kinetics for GA on zedoary starch (blue), potato starch (red), and tapioca starch (yellow). (A) Conventional and (B) inverse kinetics. Lines represent best fits of the Michaelis-Menten equations (eq. (2) or 3). (C) $^{kin}\Gamma_{max}$, and (D) Attack site density/binding density site (A/B ratio). ****, **, and * represent statistical significance with p value < 0.0001, 0.001–0.01, and 0.01–0.05, respectively.

double-helical structures and therefore introduce defects into the crystallites and disturb the crystal organization (Li, Hemar, & Zhu, 2021; Roman et al., 2020). Besides the chain length distribution of AP, AM chains, especially longer AM chains, could disrupt the formation of double helical segments and crystal structures (G. Li, Hemar, & Zhu, 2021; Zhu, 2018). This explains the lowest crystallinity of tapioca starch and a lower crystallinity of potato starch compared with zedoary starch.

Interestingly, $^{kin}\Gamma_{max}$ was also found to be negatively correlated with the short fa chains, while positively related to the long chains (fb_1 and fb_2 chain) on the surface. Our former study demonstrated that, when a substrate chain is too long or too short, GA can bind, but not catalyze the hydrolysis of the substrate chain (Tian, Wang, Liu, et al., 2023). As a result, we hypothesize that the relatively longer branches on the surface of tapioca starch potentially provide sufficient chain length to enter the active site of GA, hence GA has more attack sites on the surface of tapioca starch.

Among the starch granules with smooth surfaces in this study, we suggest that those with lower crystallinity—characteristic by having short AP chains and longer AM chains—and relatively more longer chains on the surface, contribute more attack sites for GA resulting lower enzymatic resistance.

5. Conclusion

Understanding the mechanisms underlying interfacial enzyme-catalyzed reactions is crucial for elucidating key structure controlling enzymatic degradation of starch granules. In this study, we combined interfacial kinetics and *Langmuir* adsorption isotherm analysis to explore the enzymatic resistance mechanisms of granular starches. The investigation focused on three types of starches derived from i) zedoary rhizomes, ii) potato tubers, and iii) tapioca roots. Despite all three starches exhibiting smooth granular surfaces, they displayed decreasing degrees of resistance to glucoamylase (GA) in the order zedoary > potato > tapioca starch. The enzymatic resistance to GA primarily correlated to the density of attack sites. Notably, a smooth surface acts effectively as a barrier against the ingress of digestive enzymes, but does not dictate the density of attack sites, also not correlated with the SSA. Rather, the highest crystallinity, particularly B-type crystallinity, emerges as a critical parameter in this regard. B-type crystallinity exhibited a negative correlation with GA affinity and the density of attack sites. Furthermore, the analysis revealed that the density of attack sites is predominantly influenced by the chain length on the surface of starch granules. In essence, the findings provide deeper understanding of the enzymatic hydrolysis of granular starches and the enzymatic modification of starch. These insights hold significant implications for various fields, including food science, biotechnology, and pharmaceuticals, such as preparation of new RSII by modifying the surface structure, developing RS-based delivery systems for dietary supplements, and improving the digestibility of raw starch in animal feed through enzymatic treatment, which can enhance the nutritional value and energy efficiency for livestock. From a future perspective, the kinetic analysis of additional human digestive enzymes, such as pancreatic α-amylase and α-glucosidases, can provide comprehensive information to aid in understanding the digestibility of granular starch.

CRediT authorship contribution statement

Yu Wang: Writing – review & editing, Writing – original draft, Software, Methodology, Investigation, Formal analysis, Data curation, Conceptualization. **Yu Tian:** Writing – review & editing, Writing – original draft, Software, Methodology, Investigation, Formal analysis, Conceptualization. **Zhihang Li:** Writing – review & editing, Methodology, Investigation. **Jacob Judas Kain Kirkensgaard:** Writing – review & editing, Methodology. **Birte Svensson:** Writing – review & editing,

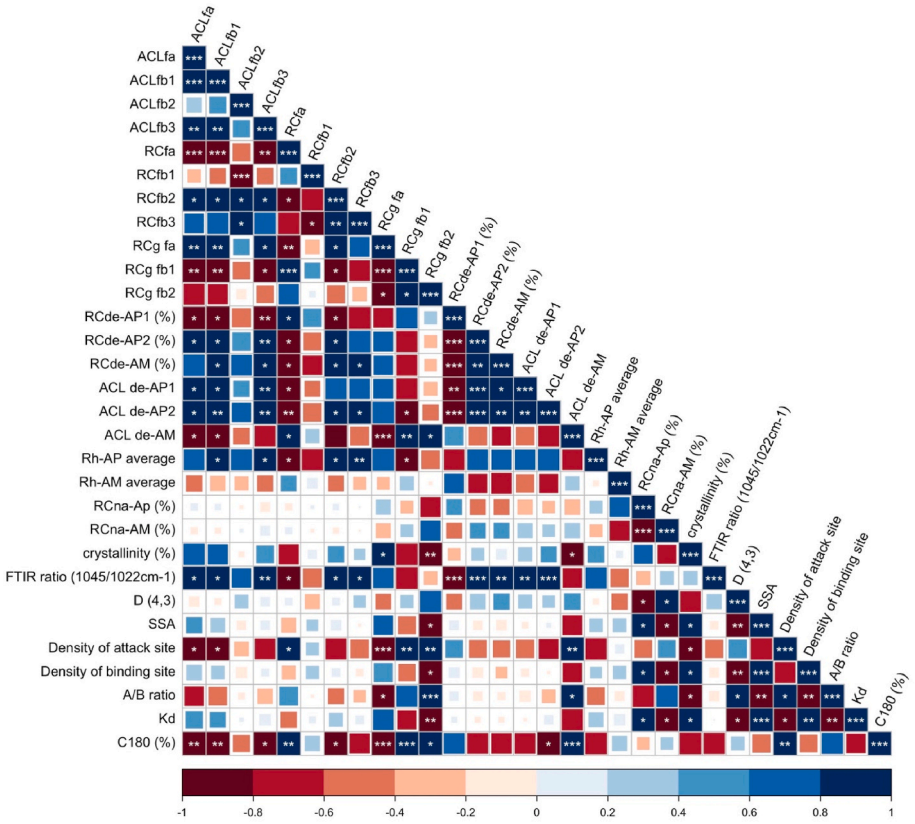

Fig. 8. Correlation analysis between the interfacial kinetic parameters and the structural parameters of different starches. ***, **, and * represent statistical significance with *p* value 0.0001–0001, 0.001–0.01, and 0.01–0.05, respectively. C180: degree of digestion after 180 min.

Supervision, Resources, Funding acquisition. **Andreas Blennow:** Writing – review & editing, Supervision, Funding acquisition, Conceptualization.

Declaration of competing interest

The authors declare that they have no competing interests.

Data availability

Data will be made available on request.

Abbreviations

A/B ratio	Attack site density/binding site density ratio
$^{ads}\Gamma_{max}$	density of binding sites
ACL	the average chain length (DP)
AM	amylose
AP	amylopectin
CLD	chain length distribution
C180	degree of digestion after 180 min
DP	degree of polymerization
$D_{4,3}$	the volume-weighted mean diameter
E_0	the enzyme load under inverse kinetics
fa	chains with DP 6–12
fb_1	chains with DP 13–24
fb_2	chains with DP 25–36
fb_3	chains with DP > 36
GA	glucoamylase
GH	glycoside hydrolase
FTIR ratio	the ratio of 1045 cm^{-1}/1022 cm^{-1} from the FTIR-ATR spectra

Acknowledgement

This work was supported by the Independent Research Fund Denmark, project BioMarch, grant #3105-00327 B (AB, BS), China Scholarship Council (CSC) grants #202003250068 (YT) and #202006790033 (YW) and the Technical University of Denmark (YW).

$^{inv}K_M$	the enzyme concentration at enzyme half-saturation under inverse kinetics
$^{inv}V_{max}$	the maximum rate under inverse kinetics
k_{cat}	turnover number under conventional kinetics
$k_{cat}/K_{1/2}$	catalytic efficiency from conventional kinetics
K_d	binding affinity
$^{kin}\Gamma_{max}$	density of attack sites
$K_{1/2}$	the mass load at substrate half-saturation under conventional kinetics
RC	relative amount
Rh	hydrodynamic radius
RS	resistant starch
S_0^{mass}	substrate mass load from conventional kinetics
V_{max}	the maximum rate under conventional kinetics

References

Abegunde, O. K., Mu, T.-H., Chen, J.-W., & Deng, F.-M. (2013). Physicochemical characterization of sweet potato starches popularly used in Chinese starch industry. *Food Hydrocolloids, 33*, 169–177.

Baldwin, A. J., Egan, D. L., Warren, F. J., Barker, P. D., Dobson, C. M., Butterworth, P. J., & Ellis, P. R. (2015). Investigating the mechanisms of amylolysis of starch granules by solution-state NMR. https://doi.org/10.1021/acs.biomac.5b00190.

Bertoft, E. (2017). Understanding starch structure: Recent progress. *Agronomy, 7*, 56. https://doi.org/10.3390/AGRONOMY7030056

Blennow, A., Bay-Smidt, A. M., Wischmann, B., Olsen, C. E., & Møller, B. L. (1998). The degree of starch phosphorylation is related to the chain length distribution of the neutral and the phosphorylated chains of amylopectin. *Carbohydrate Research, 307*, 45–54.

Blennow, A., Hansen, M., Schulz, A., Jørgensen, K., Donald, A. M., & Sanderson, J. (2003). The molecular deposition of transgenically modified starch in the starch granule as imaged by functional microscopy. *Journal of Structural Biology, 143*, 229–241. https://doi.org/10.1016/j.jsb.2003.08.009

Blennow, A., Wischmann, B., Houborg, K., Ahmt, T., Jørgensen, K., Engelsen, S. B., Bandsholm, O., & Poulsen, P. (2005). Structure function relationships of transgenic starches with engineered phosphate substitution and starch branching. *International Journal of Biological Macromolecules, 36*, 159–168. https://doi.org/10.1016/j.ijbiomac.2005.05.006

Braga, M. E. M., Moreschi, S. R. M., & Meireles, M. A. A. (2006). Effects of supercritical fluid extraction on *Curcuma longa* L. and *Zingiber officinale* R. starches. *Carbohydrate Polymers, 63*, 340–346. https://doi.org/10.1016/j.carbpol.2005.08.055

Brückner, S. (2000). Pulwin: A program for analyzing powder x-ray diffraction patterns. *Powder Diffraction, 15*, 218–219. https://doi.org/10.1017/S0885715600011118

Butterworth, P. J., Bajka, B. H., Edwards, C. H., Warren, F. J., & Ellis, P. R. (2022). Enzyme kinetic approach for mechanistic insight and predictions of in vivo starch digestibility and the glycaemic index of foods. *Trends in Food Science & Technology, 120*, 254–264. https://doi.org/10.1016/J.TIFS.2021.11.015

Cai, L., & Shi, Y. C. (2014). Preparation, structure, and digestibility of crystalline A- and B-type aggregates from debranched waxy starches. *Carbohydrate Polymers, 105*, 341–350. https://doi.org/10.1016/j.carbpol.2014.01.075

Capron, I., Robert, P., Colonna, P., Brogly, M., & Planchot, V. (2007). Starch in rubbery and glassy states by FTIR spectroscopy. *Carbohydrate Polymers, 68*, 249–259.

Carciofi, M., Blennow, A., Jensen, S. L., Shaik, S. S., Henriksen, A., Buléon, A., Holm, P. B., & Hebelstrup, K. H. (2012). Concerted suppression of all starch branching enzyme genes in barley produces amylose-only starch granules. *BMC Plant Biology, 12*, 1–16.

Cave, R. A., Seabrook, S. A., Gidley, M. J., & Gilbert, R. G. (2009). Characterization of starch by size-exclusion chromatography: The limitations imposed by shear scission. *Biomacromolecules, 10*, 2245–2253.

Cerqueira, F. M., Photenhauer, A. L., Pollet, R. M., Brown, H. A., & Koropatkin, N. M. (2020). Starch digestion by gut bacteria: Crowdsourcing for carbs. *Trends in Microbiology*. https://doi.org/10.1016/j.tim.2019.09.004

Chen, P., Wang, K., Kuang, Q., Zhou, S., Wang, D., & Liu, X. (2016). Understanding how the aggregation structure of starch affects its gastrointestinal digestion rate and extent. *International Journal of Biological Macromolecules, 87*, 28–33. https://doi.org/10.1016/j.ijbiomac.2016.01.119

Chi, C., Li, X., Huang, S., Chen, L., Zhang, Y., Li, L., & Miao, S. (2021). Basic principles in starch multi-scale structuration to mitigate digestibility: A review. *Trends in Food Science & Technology, 109*, 154–168. https://doi.org/10.1016/J.TIFS.2021.01.024

Dhital, S., Warren, F. J., Zhang, B., & Gidley, M. J. (2014). Amylase binding to starch granules under hydrolysing and non-hydrolysing conditions. *Carbohydrate Polymers, 113*, 97–107. https://doi.org/10.1016/j.carbpol.2014.06.063

Fang, K., Deng, L., Yin, J., Yang, T., Li, J., & He, W. (2022). Recent advances in starch-based magnetic adsorbents for the removal of contaminants from wastewater: A review. *International Journal of Biological Macromolecules, 218*, 909–929. https://doi.org/10.1016/J.IJBIOMAC.2022.07.175

França, D., Siqueira, G., Nyström, G., Clemens, F., Souza, C. F., & Faez, R. (2022). Charged-cellulose nanofibrils as a nutrient carrier in biodegradable polymers for enhanced efficiency fertilizers. *Carbohydrate Polymers, 296*, Article 119934.

Guo, L., Deng, Y., Lu, L., Zou, F., & Cui, B. (2019). Synergistic effects of branching enzyme and transglucosidase on the modification of potato starch granules. *International Journal of Biological Macromolecules, 130*, 499–507. https://doi.org/10.1016/j.ijbiomac.2019.02.160

Huggett, A. (1957). Enzymic determination of blood glucose. *Biochemical Journal, 66*, Article 12P.

Jane, J., Kasemsuwan, T., Leas, S., Zobel, H., & Robyt, J. F. (1994). Anthology of starch granule morphology by scanning electron microscopy. *Starch Staerke, 46*, 121–129.

Jung, K. H., Kim, M. J., Park, S. H., Hwang, H. S., Lee, S., Shim, J. H., Kim, M. J., Kim, J. C., & Lee, H. (2013). The effect of granule surface area on hydrolysis of native starches by pullulanase. *Starch/Staerke, 65*, 848–853. https://doi.org/10.1002/star.201200226

Kari, J., Andersen, M., Borch, K., & Westh, P. (2017). An inverse Michaelis-Menten approach for interfacial enzyme kinetics. *ACS Catalysis, 7*, 4904–4914. https://doi.org/10.1021/ACSCATAL.7B00838

Kari, J., Schiano-Di-Cola, C., Hansen, S. F., Badino, S. F., Sørensen, T. H., Cavaleiro, A. M., Borch, K., & Westh, P. (2020). A steady-state approach for inhibition of heterogeneous enzyme reactions. *Biochemical Journal, 447*, 1971–1982. https://doi.org/10.1042/BCJ20200083

Kulp, K., Olewnik, M., Lorenz, K., & Collins, F. (1991). Starch functionality in cookie systems. *Starch - Stärke, 43*, 53–57. https://doi.org/10.1002/star.19910430205

Lee, E. S., Shin, H., Seo, J. M., Nam, Y. D., Lee, B. H., & Seo, D. H. (2018). Effects of raw potato starch on body weight with controlled glucose delivery. *Food Chemistry, 256*, 367–372. https://doi.org/10.1016/j.foodchem.2018.02.150

Lever, M., Powell, J. C., Killip, M., & Small, C. W. (1973). A comparison of 4-hydroxy-benzoic acid hydrazide (PAHBAH) with other reagents for the determination of glucose. *The Journal of Laboratory and Clinical Medicine, 82*, 649–655.

Li, P., Dhital, S., Zhang, B., He, X., Fu, X., & Huang, Q. (2018). Surface structural features control in vitro digestion kinetics of bean starches. *Food Hydrocolloids, 85*, 343–351.

Li, H., Gilbert, R. G., & Gidley, M. J. (2021a). Molecular-structure evolution during in vitro fermentation of granular high-amylose wheat starch is different to in vitro digestion. *Food Chemistry, 362*, Article 130188. https://doi.org/10.1016/j.foodchem.2021.130188

Li, G., Hemar, Y., & Zhu, F. (2021b). Relationships between supramolecular organization and amylopectin fine structure of quinoa starch. *Food Hydrocolloids, 117*, Article 106685.

Li, H., Prakash, S., Nicholson, T. M., Fitzgerald, M. A., & Gilbert, R. G. (2016). The importance of amylose and amylopectin fine structure for textural properties of cooked rice grains. *Food Chemistry, 196*, 702–711.

Li, H., Zhai, F., Li, J., Zhu, X., Guo, Y., Zhao, B., & Xu, B. (2021c). Physicochemical properties and structure of modified potato starch granules and their complex with tea polyphenols. *International Journal of Biological Macromolecules, 166*, 521–528. https://doi.org/10.1016/j.ijbiomac.2020.10.209

Liu, M., Hao, Y., Wang, S., Li, S., Zhou, J., Zhang, L., Kang, X., Lyu, M., & Wang, S. (2024). Heterologous overproduction of a dextranase in *Bacillus subtilis* WB600 and its application in preparation of porous buckwheat starch. *Food Bioscience*, Article 103636.

Liu, X., Luan, H., Jinglin, Y., Wang, S., Wang, S., & Copeland, L. (2020). A method for characterizing short-range molecular order in amorphous starch. *Carbohydrate Polymers, 242*, Article 116405.

Miao, M., & BeMiller, J. N. (2023). Enzymatic approaches for structuring starch to improve functionality. *Annual Review of Food Science and Technology, 14*, 1–25.

Okuyama, M. (2011). Function and structure studies of GH family 31 and 97 α-glycosidases. *Bioscience, Biotechnology and Biochemistryiotechnology, and biochemistry, 75*, 2269–2277.

Pérez, S., & Bertoft, E. (2010). The molecular structures of starch components and their contribution to the architecture of starch granules: A comprehensive review. *Starch/Staerke, 62*, 389–420. https://doi.org/10.1002/star.201000013

Pinhero, R. G., Waduge, R. N., Liu, Q., Sullivan, J. A., Tsao, R., Bizimungu, B., & Yada, R. Y. (2016). Evaluation of nutritional profiles of starch and dry matter from early potato varieties and its estimated glycemic impact. *Food Chemistry, 203*, 356–366. https://doi.org/10.1016/j.foodchem.2016.02.040

Pokharel, A., Jaidka, R. K., Sruthi, N. U., & Bhattarai, R. R. (2023). Effects of incorporation of porous tapioca starch on the quality of white salted (udon) noodles. *Foods, 12*, 1662.

Policegoudra, R. S., & Aradhya, S. M. (2008). Structure and biochemical properties of starch from an unconventional source-Mango ginger (*Curcuma amada* Roxb.) rhizome. *Food Hydrocolloids, 22*, 513–519. https://doi.org/10.1016/j.foodhyd.2007.01.008

Prompiputtanapon, K., Sorndech, W., & Tongta, S. (2020). Surface modification of tapioca starch by using the chemical and enzymatic method. *Starch Staerke, 72*, Article 1900133.

Ren, F., Wang, J., Xie, F., Zan, K., Wang, S., & Wang, S. (2020). Applications of ionic liquids in starch chemistry: A review. *Green Chemistry, 22*, 2162–2183. https://doi.org/10.1039/c9gc03738a

Roman, L., Yee, J., Hayes, A. M. R., Hamaker, B. R., Bertoft, E., & Martinez, M. M. (2020). On the role of the internal chain length distribution of amylopectins during retrogradation: Double helix lateral aggregation and slow digestibility. *Carbohydrate Polymers, 246*, Article 116633.

Rosado, C. P., Rosa, V. H. C., Martins, B. C., Soares, A. C., Santos, I. B., Monteiro, E. B., Moura-Nunes, N., da Costa, C. A., Mulder, A. da R. P., & Daleprane, J. B. (2020). Resistant starch from green banana (*Musa* sp.) attenuates non-alcoholic fat liver accumulation and increases short-chain fatty acids production in high-fat diet-induced obesity in mice. *International Journal of Biological Macromolecules, 145*, 1066–1072. https://doi.org/10.1016/j.ijbiomac.2019.09.199

Schnell, S. (2014). Validity of the michaelis–menten equation–steady-state or reactant stationary assumption: That is the question. *FEBS Journal, 281*, 464–472.

Shrestha, A. K., Blazek, J., Flanagan, B. M., Dhital, S., Larroque, O., Morell, M. K., Gilbert, E. P., & Gidley, M. J. (2012). Molecular, mesoscopic and microscopic structure evolution during amylase digestion of maize starch granules. *Carbohydrate Polymers, 90*, 23–33. https://doi.org/10.1016/j.carbpol.2012.04.041

Sierks, M. R., Ford, C., Reilly, P. J., & Svensson, B. (1990). Catalytic mechanism of fungal glucoamylase as defined by mutagenesis of Asp 176, Glu 179 and Glu 180 in the enzyme from *Aspergillus awamori*. *Protein Engineering Design and Selection, 3*, 193–198.

Sim, L., Quezada-Calvillo, R., Sterchi, E. E., Nichols, B. L., & Rose, D. R. (2008). Human intestinal maltase-glucoamylase: Crystal structure of the N-terminal catalytic subunit and basis of inhibition and substrate specificity. *Journal of Molecular Biology, 375*, 782–792.

Sim, L., Willemsma, C., Mohan, S., Naim, H. Y., Pinto, B. M., & Rose, D. R. (2010). Structural basis for substrate selectivity in human maltase-glucoamylase and sucrase-isomaltase N-terminal domains. *Journal of Biological Chemistry, 285*, 17763–17770. https://doi.org/10.1074/jbc.M109.078980

Situ, W., Chen, L., Wang, X., & Li, X. (2014). Resistant starch film-coated microparticles for an oral colon-specific polypeptide delivery system and its release behaviors. *Journal of Agricultural and Food Chemistry, 62*, 3599–3609. https://doi.org/10.1021/jf500472b

Tatsumi, H., & Katano, H. (2005). Kinetics of the surface hydrolysis of raw starch by glucoamylase. *Journal of Agricultural and Food Chemistry, 53*, 8123–8127. https://doi.org/10.1021/jf050934c

Tatsumi, H., Katano, H., & Ikeda, T. (2007). Kinetic analysis of glucoamylase-catalyzed hydrolysis of starch granules from various botanical sources. *Bioscience Biotechnology & Biochemistry, 71*, 946–950. https://doi.org/10.1271/bbb.60598

Tian, Y., Li, M., Liu, X., Jane, J. lin, Guo, B., & Dhital, S. (2021). Storage temperature and time affect the enzyme resistance starch and glycemic response of cooked noodles. *Food Chemistry, 344*, Article 128702. https://doi.org/10.1016/J.FOODCHEM.2020.128702

Tian, Y., Liu, X., Judas, J., Kirkensgaard, K., Khakimov, B., Enemark-Rasmussen, K., Hebelstrup, K., Blennow, A., & Zhong, Y. (2024). Characterization of different high amylose starch granules. Part I : Multi-scale structures and relationships to thermal properties. *Food Hydrocolloids, 146*, Article 109286. https://doi.org/10.1016/j.foodhyd.2023.109286

Tian, Y., Wang, Y., Liu, X., Herburger, K., Westh, P., Møller, M. S., Svensson, B., Zhong, Y., & Blennow, A. (2023). Interfacial enzyme kinetics reveals degradation mechanisms behind resistant starch. *Food Hydrocolloids, 140*, Article 108621. https://doi.org/10.1016/j.foodhyd.2023.108621

Tian, Y., Wang, Y., Zhong, Y., Møller, M. S., Westh, P., Svensson, B., & Blennow, A. (2023). Interfacial catalysis during amylolytic degradation of starch granules: Current understanding and kinetic approaches. *Molecules, 28*, 3799.

Vamadevan, V., Blennow, A., Buléon, A., Goldstein, A., & Bertoft, E. (2018). Distinct properties and structures among B-crystalline starch granules. *Starch/Staerke, 70*, 1–12. https://doi.org/10.1002/star.201700240

Vilaplana, F., & Gilbert, R. G. (2010). Characterization of branched polysaccharides using multiple-detection size separation techniques. *Journal of Separation Science, 33*, 3537–3554.

Wang, Z., Hu, Z., Deng, B., Gilbert, R. G., & Sullivan, M. A. (2022). The effect of high-amylose resistant starch on the glycogen structure of diabetic mice. *International Journal of Biological Macromolecules, 200*, 124–131. https://doi.org/10.1016/j.ijbiomac.2021.12.071

Wang, Y., Svensson, B., Henrissat, B., & Møller, M. S. (2023). Functional roles of N-terminal domains in pullulanase from human gut *Lactobacillus acidophilus*. *Journal of Agricultural and Food Chemistry, 71*, 18898–18908. https://doi.org/10.1021/acs.jafc.3c06487

Wang, Y., Tian, Y., Christensen, S. J., Blennow, A., Svensson, B., & Møller, M. S. (2024). An enzymatic approach to quantify branching on the surface of starch granules by interfacial catalysis. *Food Hydrocolloids, 146*, Article 109162. https://doi.org/10.1016/j.foodhyd.2023.109162

Wang, Y., Tian, Y., Zhong, Y., Suleiman, M. A., Feller, G., Westh, P., Blennow, A., Møller, M. S., & Svensson, B. (2023). Improved hydrolysis of granular starches by a psychrophilic α-amylase starch binding domain-fusion. *Journal of Agricultural and Food Chemistry, 71*, 9040–9050. https://doi.org/10.1021/acs.jafc.3c01898

Warren, F. J., Royall, P. G., Gaisford, S., Butterworth, P. J., & Ellis, P. R. (2011). Binding interactions of α-amylase with starch granules: The influence of supramolecular structure and surface area. *Carbohydrate Polymers, 86*, 1038–1047. https://doi.org/10.1016/j.carbpol.2011.05.062

Wei, T., Simko, V., Levy, M., Xie, Y., Jin, Y., & Zemla, J. (2017). Package 'corrplot. *Statistician, 56*, e24.

Xiao, Y., Kuang, J., Qi, X., Ye, Y., Wu, Z., Chen, J., & Lu, W. (2018). A comprehensive investigation of starch degradation process and identification of a transcriptional activator Mab HLH 6 during banana fruit ripening. *Plant Biotechnology Journal, 16*, 151–164.

Xu, C., Li, C., Li, E., & Gilbert, R. G. (2024). Insights into wheat-starch biosynthesis from two-dimensional macromolecular structure. *Carbohydrate Polymers, 337*, Article 122190. https://doi.org/10.1016/j.carbpol.2024.122190

Yu, W., Li, H., Zou, W., Tao, K., Zhu, J., & Gilbert, R. G. (2019). Using starch molecular fine structure to understand biosynthesis-structure-property relations. *Trends in Food Science & Technology, 86*, 530–536.

Zhang, B., Dhital, S., & Gidley, M. J. (2015). Densely packed matrices as rate determining features in starch hydrolysis. *Trends in Food Science & Technology, 43*, 18–31.

Zhang, Z., Fan, X., Ma, H., Li, C., Li, E., & Gilbert, R. G. (2021). Characterization of the baking-induced changes in starch molecular and crystalline structures in sugar-snap cookies. *Carbohydrate Polymers, 256*, Article 117518. https://doi.org/10.1016/j.carbpol.2020.117518

Zhang, L., Zhao, Y., Hu, W., Qian, J. Y., Ding, X. L., Guan, C. R., Lu, Y. Q., & Cao, Y. (2018). Multi-scale structures of cassava and potato starch fractions varying in granule size. *Carbohydrate Polymers, 200*, 400–407. https://doi.org/10.1016/j.carbpol.2018.08.022

Zhong, Y., Herburger, K., Kirkensgaard, J. J. K., Khakimov, B., Hansen, A. R., & Blennow, A. (2021a). Sequential maltogenic α-amylase and branching enzyme treatment to modify granular corn starch. *Food Hydrocolloids, 120*, Article 106904. https://doi.org/10.1016/J.FOODHYD.2021.106904

Zhong, Y., Li, Z., Qu, J., Bertoft, E., Li, M., Zhu, F., Blennow, A., & Liu, X. (2021b). Relationship between molecular structure and lamellar and crystalline structure of rice starch. *Carbohydrate Polymers, 258*, Article 117616.

Zhong, Y., Xu, J., Liu, X., Ding, L., Svensson, B., Herburger, K., Guo, K., Pang, C., & Blennow, A. (2022). Recent advances in enzyme biotechnology on modifying gelatinized and granular starch. *Trends in Food Science & Technology, 123*, 343–354. https://doi.org/10.1016/j.tifs.2022.03.019

Zhu, F. (2018). Relationships between amylopectin internal molecular structure and physicochemical properties of starch. *Trends in Food Science & Technology, 78*, 234–242.

Zhu, L., Jones, C., Guo, Q., Lewis, L., Stark, C. R., & Alavi, S. (2016). An evaluation of total starch and starch gelatinization methodologies in pelleted animal feed. *Journal of Animal Science, 94*, 1501–1507.

Zhu, H., Wang, C., Wang, Y., Yu, J., Copeland, L., & Wang, S. (2024). Novel type of slowly digested starch complex with antioxidant properties. *Biomacromolecules,, 25*, 2914–2924.